Molecular Biology of the Cell
Vol. 17, 1331–1343, March 2006

The *Arabidopsis thaliana PARTING DANCERS* Gene Encoding a Novel Protein Is Required for Normal Meiotic Homologous Recombination[D]

Asela J. Wijeratne,*†‡ Changbin Chen,†‡ Wei Zhang,†‡ Ljudmilla Timofejeva,†§ and Hong Ma*†

*Intercollege Graduate Program in Plant Physiology and †Department of Biology and the Huck Institutes of the Life Sciences, The Pennsylvania State University, University Park, PA 16802; and §Department of Gene Technology, Tallinn University of Technology, Tallinn 19086, Estonia

Submitted September 29, 2005; Revised December 2, 2005; Accepted December 27, 2005
Monitoring Editor: Kerry Bloom

Recent studies of meiotic recombination in the budding yeast and the model plant *Arabidopsis thaliana* indicate that meiotic crossovers (COs) occur through two genetic pathways: the interference-sensitive pathway and the interference-insensitive pathway. However, few genes have been identified in either pathway. Here, we describe the identification of the *PARTING DANCERS* (*PTD*) gene, as a gene with an elevated expression level in meiocytes. Analysis of two independently generated transferred DNA insertional lines in *PTD* showed that the mutants had reduced fertility. Further cytological analysis of male meiosis in the *ptd* mutants revealed defects in meiosis, including reduced formation of chiasmata, the cytological appearance of COs. The residual chiasmata in the mutants were distributed randomly, indicating that the *ptd* mutants are defective for CO formation in the interference-sensitive pathway. In addition, transmission electron microscopic analysis of the mutants detected no obvious abnormality of synaptonemal complexes and apparently normal late recombination nodules at the pachytene stage, suggesting that the mutant's defects in bivalent formation were postsynaptic. Comparison to other genes with limited sequence similarity raises the possibility that *PTD* may present a previously unknown function conserved in divergent eukaryotic organisms.

INTRODUCTION

During meiotic prophase I, homologous chromosomes (homologues) interact through pairing, synapsis, and recombination, which are required for the proper segregation of homologues during subsequent stages of meiosis. Such interactions begin with the pairing of two homologues, followed by the polymerization of the synaptonemal complex (synapsis) between the homologues (Page and Hawley, 2004). Under a transmission electron microscope (TEM), the synaptonemal complex (SC) can be observed as a structure with three parallel filaments: two outer lateral elements and one central element (Page and Hawley, 2004). In addition, electron-dense ovoid structures (late recombination nodule, or LN) can be seen associated with the SC (Page and Hawley, 2004). LNs correlate with sites of meiotic crossovers (COs) (Page and Hawley, 2004). During late stages of the meiotic prophase I, SCs disassemble (desynapsis). By this time, homologue recombination has been completed, and the resulting COs can be seen cytologically as chiasmata. The attached homologues known as bivalents align at the metaphase plate, ensuring the correct segregation of homologues during anaphase I. The COs, along with cohesion between sister chromatids, are important for the maintenance of homologue association until the transition from metaphase I to anaphase I is complete (Page and Hawley, 2003).

Although the molecular process of recombination is not yet fully understood, studies in yeast and other organisms have led to the double-strand break repair (DSBR) model (Szostak *et al*., 1983). According the DSBR model, recombination is initiated by a double-strand break (DSB) generated by the SPO11 protein, originally discovered in the budding yeast *Saccharomyces cerevisiae* (Esposito and Esposito, 1969; Keeney, 2001; Lichten, 2001). Homologues of SPO11 have been identified in a wide range of other organisms, including other fungi, plants, and animals, suggesting that the mechanism of recombination initiation is highly conserved (Dernburg *et al*., 1998; McKim and Hayashi-Hagihara, 1998; Keeney *et al*., 1999; Romanienko and Camerini-Otero, 1999; Celerin *et al*., 2000; Grelon *et al*., 2001). After DSBs are formed, they are processed by the MRE11–RAD50–XRS2 protein complex to form 3′OH single-stranded ends (Symington, 2002). RAD51, a homologue to the bacterial recombinase RecA, and its meiotic paralog DMC1 then are localized to the 3′ single-stranded-tails to facilitate single strand invasion of intact duplexes (Petukhova *et al*., 2000; Sung *et al*., 2003).

According to the current understanding, the early interaction between the invading strand and intact duplex is transient and can have three different fates (Bishop and

This article was published online ahead of print in *MBC in Press* (http://www.molbiolcell.org/cgi/doi/10.1091/mbc.E05–09–0902) on January 4, 2006.

[D] The online version of this article contains supplemental material at *MBC Online* (http://www.molbiolcell.org).

‡ These authors contributed equally to this work.

Address correspondence to: Hong Ma (hxm16@psu.edu).

Abbreviations used: CO, crossover; dHJ, double Holliday junction; DSB, double-strand break; LN, late recombination nodule; NCO, noncrossover; RT, reverse-transcription; T-DNA, transferred DNA; TEM, transmission electron microscope.

Zickler, 2004). The interactions can be processed to form noncrossovers (NCOs), or they can be processed through one of two genetically separate pathways for CO formation (Bishop and Zickler, 2004; Börner *et al*., 2004). One of the CO pathways is dependent on the two eukaryotic homologues of the bacterial MutS protein, MSH4 and MSH5, whereas the other CO pathway is dependent on the heterodimeric endonuclease with the MUS81 and MMS4/EME1 subunits (de los Santos *et al*., 2003; Hollingsworth and Brill, 2004). In many organisms, the presence of a CO inhibits the formation of a second CO nearby between the same pair of homologues, a phenomenon known as interference (Hillers, 2004). The MSH4–MSH5-dependent pathway forms COs that show interference, whereas the MUS81–MMS4/EME1-dependent COs do not show interference (de los Santos *et al*., 2003; Bishop and Zickler, 2004; Hollingsworth and Brill, 2004). In addition, the numbers of COs formed through these two pathways vary in different organisms (Hollingsworth and Brill, 2004). For example, in budding yeast and *Arabidopsis* the MSH4–MSH5-dependent pathway accounts for the majority of COs, whereas the MUS81–MMS4/EME1 pathway accounts for most, if not all, of the COs generated in fission yeast (Copenhaver *et al*., 2002; de los Santos *et al*., 2003; Bishop and Zickler, 2004; Hollingsworth and Brill, 2004).

There is considerable information on the interference-sensitive pathway. In yeast, the initial interaction between the invading stand and the intact duplex proceeds to form a stable intermediate, known as the single strand invasion intermediate (SEI) (Bishop and Zickler, 2004). Further DNA synthesis and ligation, through the second end capture (SEC) intermediates, leads to the formation of the recombinant intermediate, known as the double Holliday junction (dHJ). In principle, resolution of dHJ can give rise to either COs or NCOs, but recent results in *S. cerevisiae* indicate that dHJs tend to resolve only to form COs (Bishop and Zickler, 2004). The MSH4 and MSH5 proteins form a heterodimer and seem to function in stabilizing and preserving CO intermediates (Pochart *et al*., 1997; Bocker *et al*., 1999; Colaiacovo *et al*., 2003; Snowden *et al*., 2004). The *msh4* and *msh5* mutants in *S. cerevisiae* show a reduction in COs without affecting NCOs (Ross-Macdonald and Roeder, 1994; Hollingsworth *et al*., 1995). More specifically, the budding yeast *msh5* mutant shows defects in the conversion of DSBs into SEI and in the formation of dHJ (Börner *et al*., 2004). Similarly, a mutant in the *Arabidopsis* homologue of *MSH4*, *atmsh4*, shows a dramatic reduction of interference-sensitive COs, whereas the formation of interference-insensitive COs occurs at the expected levels (Higgins *et al*., 2004), indicating that the interference-sensitive pathway in *Arabidiopsis* also requires *MSH4*. MSH4 and MSH5 homologues in mammals are also important for meiosis (de Vries *et al*., 1999; Kneitz *et al*., 2000), although analysis of CO formation in mutant mice have not yet been described. In addition, statistical modeling suggests that humans may also have two CO pathways with only one forming interference-sensitive COs (Housworth and Stahl, 2003).

In addition, the *S. cerevisiae* mutant *mer3* and the *Arabidopsis* mutant (*atmer3/rck*) in the *MER3* homologue are impaired in the formations of COs via the interference-sensitive pathway (Nakagawa and Ogawa, 1999; Chen *et al*., 2005; Mercier *et al*., 2005). Furthermore, a recent study has shown that MER3, which is a DNA helicase, is involved in DNA heteroduplex extension in the 3′–5′ direction in SEC intermediates (Mazina *et al*., 2004). Therefore, the interference-sensitive CO pathway seems to be conserved in yeast, plants, and probably mammals, involving at least the MSH4/MSH5 heterodimer and likely the MER3 DNA helicase.

However, relatively little is known about the protein(s) involved in dHJ resolution in eukaryotes. During dHJ resolution, DNA strands need to be cleaved and ligated in a specific orientation to form COs (Heyer *et al*., 2003). In prokaryotes, two classes of proteins, represented by the *Escherichia coli* RuvC resolvase and the archeal Hjc nuclease serve as Holliday junction resolvases (Kvaratskhelia *et al*., 2001; Lilley and White, 2001; Heyer *et al*., 2003; Parker and White, 2005). In *Drosophila melanogaster*, *mei-9* and *ercc1* mutations lead to a reduction in CO formation (Baker and Carpenter, 1972; Carpenter, 1979, 1982; Sekelsky *et al*., 1995; Radford *et al*., 2005). *MEI-9* encodes a homologue of the mammalian XPF structure-specific DNA endonuclease that is critical for DNA excision repair (Sekelsky *et al*., 1995; Sijbers *et al*., 1996; de Laat *et al*., 1998; Yildiz *et al*., 2004). Furthermore, *mei-9* meiocytes exhibit unaltered distribution, frequency, and morphology of LNs (Carpenter, 1979), suggesting that MEI-9 acts at a stage after LN formation, possibly at the dHJ resolution step. The *Drosophila* ERCC1 is a homologue of mammalian ERCC1, which forms a complex with XPF (Sijbers *et al*., 1996; de Laat *et al*., 1998; Sekelsky *et al*., 2000). In addition, recent studies revealed that RAD51 paralogs might also be involved at dHJ resolution (Yokoyama *et al*., 2003, 2004; Liu *et al*., 2004). However, it is expected that more genes need to be identified to fully understand the molecular process of homologous recombination during meiosis.

With the rapid advancements of *Arabidopsis* molecular and cell biological studies because of readily available genetic and cytological tools, analysis in *Arabidopsis* has led to novel findings in the meiotic process (Ma, 2005). For example, the isolation and analysis of the *solo dancers* (*sds*) mutant indicates that a novel cyclin protein, SDS, is required for normal recombination and bivalent formation (Azumi *et al*., 2002; Wang *et al*., 2004). In addition, analysis of the *Arabidopsis* mutant *meiotic prophase aminopeptidase1* (*mpa1*) indicates that a puromycin-sensitive aminopeptidase is involved in meiotic recombination (Sanchez-Moran *et al*., 2004). Furthermore, plant-specific meiotic genes, such as *SWI1*, have been identified that have no known functional homologues in other organisms (Mercier *et al*., 2001, 2003). Reverse genetic studies have also demonstrated the importance of homologues of known meiotic recombination genes in *Arabidopsis* meiosis (Grelon *et al*., 2001; Bleuyard and White, 2004; Li *et al*., 2004, 2005; Mercier *et al*., 2005). These studies indicate that meiosis uses both conserved and divergent mechanisms.

Here, we report the identification of an *Arabidopsis* gene, *PARTING DANCERS* (*PTD*), which is involved specifically in meiotic prophase I. We present data from cytological and quantitative cytogenetic studies showing that *ptd* meiocytes exhibit reduced levels of crossover formation. The distribution of remaining crossovers suggests that the *PTD* gene is important for the promotion of interference-sensitive crossovers. The *PTD* gene seems to function at a postsynaptic step, indicating a role in late stages of crossover pathway. Furthermore, *PTD* encodes a protein with limited sequence similarity to ERCC1 proteins and other proteins, suggesting possible mechanisms for *PTD* function.

MATERIALS AND METHODS

Plant and Growth Conditions

Both the wild-type and the *ptd* mutant plants carrying a transferred DNA (T-DNA) insertion, SALK_127477 (*ptd-1*) and SAIL_567_D09 (*ptd-2*), were of the Columbia ecotype unless otherwise indicated. All plants were grown under long-day conditions (16-h day and 8-h night) in a growth room at an average of 18–22°C or in a greenhouse.

Table 1. Sequence information for oligonucleotides used

Primer name	Sequence
oMC571	TCCCAGAATCGCTAAGATTGCC
oMC572	CCTTTCCCTTAAGCTCTG
oMC1607	TCAAAACACATATCGCCTA
oMC1608	GTAATGTGGAGCGTATGGA
oMC1735	ATCATCAAGTTTCGTCACCTCTC
oMC1736	TCTGTGTTTGCTAAAATGTCTTC
oMC1863	TAGACGGTTTTTCGCCCTTTGACG
oMC1996	TCCGCCAAGATTTTCGAATTTCT
oMC1998	AAACAAGTGTGGTCATCTATTGTG
oMC1887	ACAAAAGCAATAGAAACACCTCCAC
oMC1911	GACAAATCTGATGAAGATGTTTG
oMC1912	TGCTTATCTGTGTTGTCGGAAAT
oMC2009	TAGCATCTGAATTTCATAACCAATCTCGATACAC

Phenotypic Analysis

Plants were photographed using Sony digital camera DSC-F828 (Sony, Tokyo, Japan). Dissected tetrads were stained with 0.01% toluidine blue. Pollen grains were stained with Alexander's solution (Alexander, 1969) to test for pollen viability. The images were obtained using a Nikon dissecting microscope (Nikon, Tokyo, Japan) with an Optronics digital camera (Optronics, Goleta, CA). Wild-type and mutant inflorescences were collected, and chromosome spreads were prepared as described by Ross *et al*. (1996) and stained with 1 μg/ml 4′,6-diamidino-2-phenylindole (DAPI). Images of chromosome spreads were obtained using a Nikon Eclipse E800 microscope (Nikon) and a Hamamatsu digital camera (Hamamatsu Photonics, Hamamatsu, Japan). The images were edited using Photoshop 7.0 (Adobe Systems, Mountain View, CA). Number of chiasmata was counted from diakinesis images in a way similar to that described previously (Sanchez Moran *et al*., 2001). Transmission electron microscopy was carried out as described previously (Li *et al*., 2004). All statistical analyses were carried out as described previously (Zar, 1974).

PCR and Sequencing of T-DNA Insertion Sites

All primer sequences used here are listed in Table 1. Genomic DNAs were extracted from rosette leaves using 2× CTAB buffer [2% (wt/vol) cetyltrimethyl-ammonium bromide, 1.4 M NaCl, 100 mM Tris-HCl, pH 8.0, and 20 mM EDTA]. PCR was used to identify plants that were homozygous and heterozygous for one of the two T-DNA insertions, SALK_127477 (*ptd-1*) and SAIL_567_D09 (*ptd-2*). For the SALK_127447 line, the wild-type allele was amplified using primers oMC1607 and oMC1608, and the mutant allele was amplified using oMC1607 and oMC1863, a primer specific for the T-DNA left border. For the SAIL_567_D09 line, the wild-type allele was amplified using oMC1911 and oMC1912, and the mutant allele was amplified using a gene-specific primer oMC1911 and the T-DNA left border primer oMC2009. The products from oMC1607/oMC1863 or oMC1911/oMC2009 were purified and sequenced to confirm their identity.

Reverse Transcription (RT)-PCR

RT–PCR was performed using ~1 μg of total RNA from wild-type (Landsberg *erecta* ecotype) roots, stems, leaves, stage 12 flowers, and young inflorescences. The RNAs were treated with RNase-free DNase I, followed by the inactivation of the DNase I. The RNAs were then used to synthesize the cDNA using Superscript II (Invitrogen, Carlsbad, CA) and oligo(dT) according to manufacturer's instructions. These cDNAs were later used as template for RT-PCR using *PTD*-specific primers oMC1735 and oMC1887. As a control the same cDNAs were used to amplify the *APT1* gene (oMC571 and oMC572) encoding the adenine phosphoribosyltransferase (Moffatt *et al*., 1994). PCR was carried out under standard conditions using 10 pmol of each primer and 30 cycles (for either *APT1* or *PTD*) of 94°C for 30 s, 55°C for 45 s, and 72°C for 45 s.

To estimate the RNA expression level in mutant plants, RNA was extracted from inflorescences (containing buds younger than stage 11 flowers) of mutant plants homozygous for one of the T-DNA insertions and wild-type plants as a control. cDNA was synthesized as described above, and RT-PCR was performed with primer combinations of oMC1996 and oMC1998, oMC1735 and oMC1736, or oMC1735 and oMC1887. Positions of these PCR primers are shown in Figure 2. To confirm the *PTD* coding region, a cDNA fragment was obtained by RT-PCR using RNA from wild-type young inflorescence with oMC1996 and oMC1998 and was cloned into the pGEM-T vector (Promega, Madison, WI) (plasmid pMC2974) and sequenced.

RNA In Situ Hybridization

Nonradioactive RNA in situ hybridization was performed essentially as described previously (Xu *et al*., 2002). Wild-type inflorescences were fixed in the formol-acetic-alcohol fixative for at least 2 h at room temperature and then dehydrated, cleared, and embedded in paraffin (Fisher, Hampton, NH). Sections (10 μm in thickness) were made using a Shandon Finesse (Thermo Electron, Pittsburgh, PA) microtome and mounted onto slides. All slides were dewaxed with Histoclear, treated with protein kinase for 30 min, and then dehydrated and baked at 42°C for at least 2 h. A *PTD* cDNA fragment was amplified with gene-specific primers oMC1735 and oMC1736 and cloned into the pGEM-T vector (Promega) to yield plasmid pMC2913. The *PTD* antisense and sense RNAs were labeled with digoxigenin (DIG) through in vitro transcription of linearized pMC2913, using enzymes *Spe*I and *Nco*I, respectively. The sections were hybridized with the RNA probes, and hybridization signals were detected using anti-DIG antibodies conjugated with alkaline phosphatase and nitro blue tetrazolium chloride/5-bromo-4-chloro-3-indolyl phosphate. Images were taken using a SPOT II RT camera (Diagnostic Instruments, Sterling Heights, MI) and were edited using Photoshop 7.0 (Adobe Systems).

Sequence Analysis

Unless mentioned otherwise all homologous protein sequences were obtained using National Center for Biotechnology Information HOMOLOGENE function (http://www.ncbi.nlm.nih.gov/entrez/query.fcgi?DB = homologene). All sequence alignment was done using the MUSCLE sequence alignment program and further modified using GeneDoc (http://www.psc.edu/biomed/genedoc) (Nicholas *et al*., 1997; Edgar, 2004). Phylogenetic analyses of protein sequences were performed using *MEGA* version 3.0 software (Kumar *et al*., 2004) with default settings except for the following parameters: 1) for parsimony analysis, 500 bootstrap replicates, seed = 33,000; and 2) for Neighbor-Joining analysis, 10,000 bootstrap replicates, seed = 63,695 and pairwise deletion.

RESULTS

PTD *Is Expressed in Male Meiocytes and Other Cells in Vegetative and Floral Organs*

To identify genes that potentially function in male meiosis, microarray expression profiles of *Arabidopsis* meiotic-stage anthers were generated (Zhang, unpublished data). One gene, At1g12790, which was originally annotated as being weakly similar to bacterial DNA ligases with nonspecific DNA binding, was expressed in stage 4–6 anthers (Zhang, unpublished data). According to our published microarray data, At1g12790 expression was also detected in all organs tested, including young inflorescences (Zhang *et al*., 2005). This locus was named *PTD* for the meiotic defects of T-DNA insertion mutants in this gene (see below).

To verify the microarray results, we performed semiquantitative RT-PCR with *PTD*-specific primers and found that *PTD* was expressed at similar levels in both vegetative and reproductive organs, including anthers near the stage of meiosis (Figure 1A). To determine the *PTD* spatial expression pattern in reproductive tissues, nonradioactive in situ hybridization with inflorescence sections was carried out using an antisense *PTD* probe. Signals could be observed in early stages of floral meristem (Figure 1B). In addition, in the mature flower, the *PTD* signals were restricted to the reproductive organs stamens and carpels (Figure 1C). In the stamen, strong signals were observed in the male meiocytes and in tapetal cells, which surround the male meiocytes (Figure 1C). Moreover, signals were detected in mature pollen grains (Figure 1E). In the carpel, the *PTD* signals were present in developing ovules (Figure 1D) and in developing embryos (our unpublished data). These results indicate that *PTD* is expressed in the meiocytes and other dividing cells. In addition, we detected *PTD* expression in vegetative organs including leaves, stem, and roots.

Identification and Analysis of T-DNA Insertions in PTD

To characterize the function of *PTD*, we obtained two lines with a T-DNA insertion in the gene from the SIGnAL and SAIL collections (Sessions *et al*., 2002; Alonso *et al*., 2003), SALK_127447 and SAIL_567_D09 and were confirmed to have insertions in *PTD*. These lines showed reduced fertility (see below). The mutant alleles in these two lines were

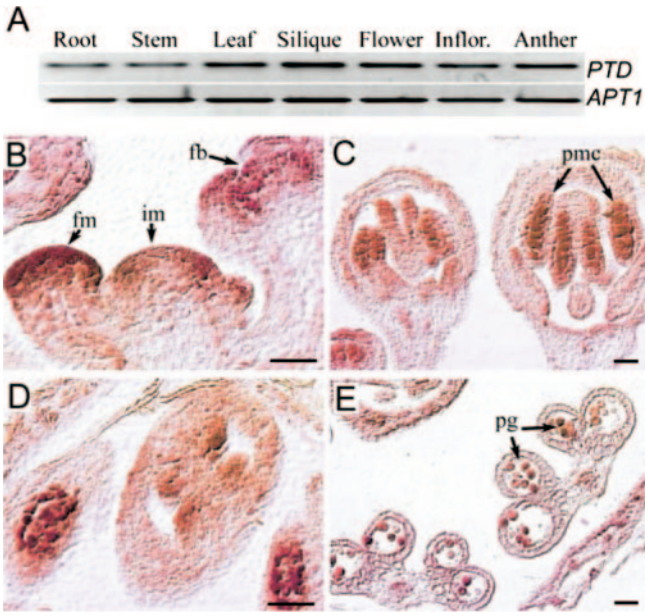

Figure 1. The expression patterns of *PTD*. (A) RT-PCR analyses of the *PTD* mRNA expression in wild-type root, stem, cauline leaf, silique, stage-12 flower, inflorescence, and anthers at stages 4–6. (B) *PTD* was expressed in the wild-type meristem and young flower buds. (C) A possible stage 5/6 (flower stage 9) wild-type anther showing *PTD* signal in the male meiocytes and tapetal layer. (D) A cross-section of a flower at stages 8–9 with developing ovules and anthers. (E) Anthers with mature pollen grains. Strong signals are associated some pollen grains. im, inflorescence meristem; fm, floral meristem; fb, a stage 4 flower bud; pmc, pollen mother cells; and pg, pollen grains. Bar, 20 μm.

named *ptd-1* (SALK_127447) and *ptd-2* (SAIL_567_D09). Plants that showed the reduced fertility were genotyped using PCR and were homozygous for the T-DNA insertion (hereafter, plants that are homozygous for either one of the T-DNA insertion will be referred as *ptd* mutant unless mentioned otherwise).

Plants heterozygous for the T-DNA insertion were phenotypically normal, indicating that the mutations are recessive. The progenies of heterozygous plants for either mutant alleles segregated for mutant to normal phenotypes in a 1:3 ratio as expected for single Mendelian recessive mutations (*ptd-1*, 187: 637 mutant:normal; *ptd-2*, 37:114 mutant:normal). To test for linkage between the T-DNA insertions and mutant phenotypes, the genotypes of these segregating populations were determined using gene-specific and T-DNA specific primers (see *Materials and Methods*). For *ptd-1*, 60 mutant plants were all *ptd-1/ptd-1*; among 48 normal plants tested, 12 were *PTD/PTD* and 36 were *PTD/ptd-1*. For *ptd-2*, 35 mutant plants were *ptd-2/ptd-2*, whereas 12 of the 22 normal plants were *PTD/PTD* with the remaining 10 being *PTD/ptd-2*. These results indicate that the *ptd-1* and *ptd-2* insertions were tightly linked to the mutant phenotype. Furthermore, *ptd-1/ptd-2* heterozygous plants were generated by crosses between *PTD/ptd-1* and *PTD/ptd-2* plants and showed similar phenotypes to those of *ptd-1* and *ptd-2* plants (including the meiotic chromosomal morphology discussed below). Because the *ptd-1* and *ptd-2* alleles were identified from independently generated T-DNA collections, these results strongly support the conclusion that the insertions in the *PTD* gene caused the mutant phenotypes.

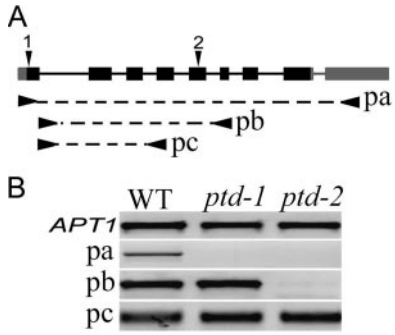

Figure 2. The *PTD* gene structure and mRNA expression in the wild type and the two mutants. (A) A diagram showing *PTD* (At1g12790) locus with the exon/intron organization of *PTD*. Solid boxes indicate exons, including full coding (black) and untranslated regions (gray). The position of the T-DNA insertion sites of the *ptd-1* and *ptd-2* alleles are indicated by black arrowhead 1 and 2. Underneath the structure, arrow-dash bars-arrows indicate the approximate positions of different primers used for RT-PCR: pa, oMC1996/oMC1998; pb, oMC1735/oMC1736; and pc, oMC1735/oMC1887. (B) Results for RT-PCR with primer pairs of pa, pb, and pc. The *APT1* control is indicated.

Using gene-specific and T-DNA left border primers, we confirmed that the SALK_127447 insertion was within the first exon, 40 base pairs downstream of the start codon, whereas the SAIL_567_D09 insertion was in the fifth exon, 430 bp downstream of start codon and in both T-DNA insertions, the left border was oriented toward the 3′ end (Figure 2A). RT-PCR of the entire coding region indicated that the *PTD* transcripts were detectable only in the wild-type young inflorescence but were not in inflorescences of either *ptd* mutants even after 40 PCR cycles. However, RT-PCR with primers that amplify a region downstream of the SALK_127447 insertion but upstream of the SAIL_567_D09 insertion showed comparable levels of *PTD* mRNA in wild-type, *ptd-1* and *ptd-2* young inflorescences (Figure 2B). These results suggest that, although T-DNA insertions might have disrupted the synthesis of the full-length *PTD* mRNA, there can be truncated versions of mRNA in both mutant alleles.

The ptd *Mutants Have Reduced Fertility and Are Defective in Meiosis*

We found that the vegetative growth in the *ptd* mutant plants was normal under standard growth conditions. In particular, the number of rosette leaves, cauline leaves, and biomass were similar to those of wild-type plants grown under the same growth conditions (Figure 3, A and B). In addition, the mutant and wild-type flowers had similar sepals and petals. However, the mutant plants (Figure 3B) produced shorter siliques with fewer seeds than the wild type (Figure 3A). The average number of seeds was approximately three per seedpod in *ptd-1* (n = 42) and *ptd-2* (n = 83), compared with 42 seeds per seedpod (n = 29) in the wild type.

Consistent with the reduced fertility, *ptd* anthers showed reduced pollen production compared with wild-type anthers (Figure 3, C and D). Furthermore, the anthers of mutant plants stained with Alexander's staining showed a large number of dead pollen grains, whereas wild-type anthers stained with the same stain showed little, if any, dead pollen (Figure 3, G and H). To ascertain the cause of the defect in pollen production in the *ptd* mutant, we stained the tetrads from both wild type and the mutant with toluidine blue.

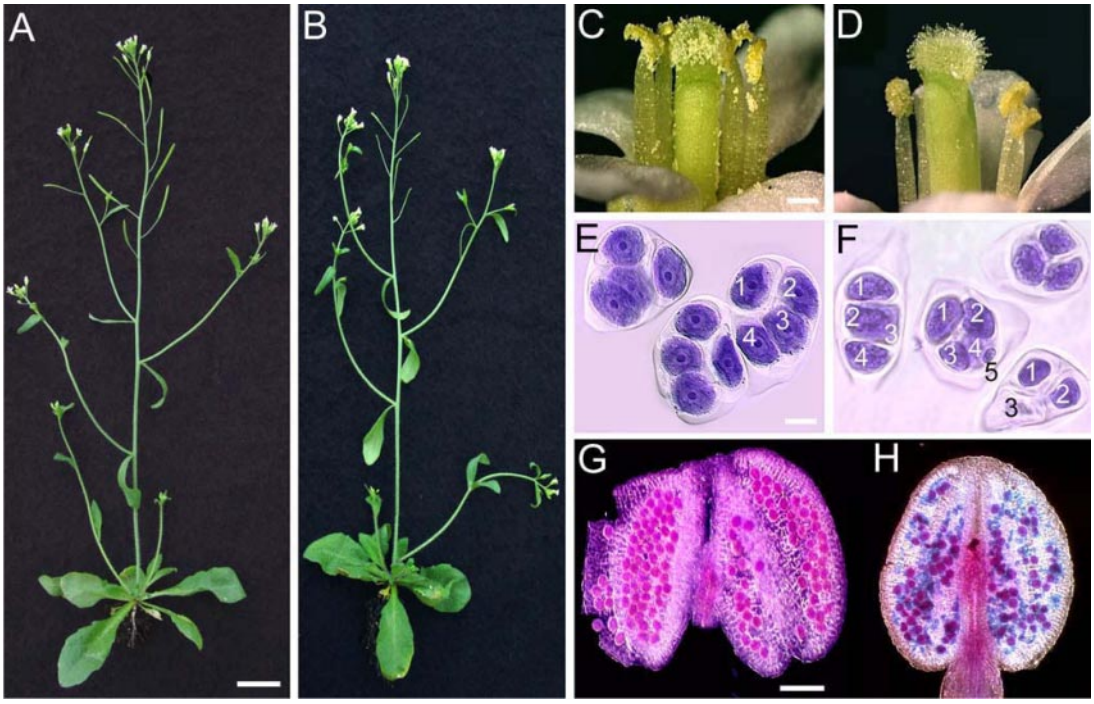

Figure 3. Phenotypes of the wild type and the *ptd-1* mutant. (A) A wild-type plant showing normal vegetative growth and normal siliques. (B) A mutant plant showing similar shape of the wild type with no detectable defects on vegetative growing but with shorter siliques. (C) A portion of a wild-type flower. (D) A portion of mutant flower with floral organs similar to the wild type except a fewer pollen grains on anthers. (E) Tetrads from a wild-type anther with four microspores. (F) Tetrads from the mutant anther with varied numbers of microspores. (G) A wild-type anther with functional pollen grains stained in red. (H) A mutant anther with fewer functional pollen grains stained with red and nonfunctional pollen grains stained with dark green. Bars, 1 cm (A and B), 200 μm (C and D), 10 μm (E and F), and 50 μm (G and H).

Completion of meiosis in wild-type plants produces tetrads with four spores, whereas the mutant plants produced polyads with two to eight spores, indicating a meiotic defect and possibly chromosome missegregation during male meiosis (Figure 3, E and F). An examination of the surface of the stigma in *ptd* flowers did not reveal any abnormality. However, the number of seeds produced by the *ptd-1* flowers whose stigma were pollinated by wild-type pollen grains was not significantly different from the number of seeds produced by self-pollinated mutant plants (24 crosses, average seed set two seeds per silique). Therefore, the *ptd* mutations seem to be defective in female reproduction as well.

ptd Meiocytes Contained a Reduced Number of Interference-sensitive Chiasmata

To obtain further insight into the meiosis of the *ptd* mutant, male meiosis in the mutant and wild type was analyzed by staining meiotic chromosome spreads with DAPI (Figure 4). The wild-type cells showed the characteristic chromosome behaviors of meiosis as described previously (Figure 4, A–D and M–P) (Ross *et al*., 1996). In the wild type, at leptotene, chromosomes started to condense and can be seen as thin treads (Figure 4A). During zygotene, chromosomes continue to condense, began to synapse, and could be seen to concentrate to one side of the nucleus (Figure 4B). During pachytene, completely synapsed chromosomes look like thick threads (Figure 4C). At diplotene, chromosomes have desynapsed, and homologues remain attached to each other only at the chiasmata (Figure 4D). During diakinesis, chromosomes contract length wise to produce highly condensed bivalents (Figure 4M).

In both mutant alleles, under the light microscope, no significant abnormality of the chromosome behaviors from leptotene to pachytene was observed (Figure 4, E–G and I–K). It was also difficult to see any defect at diplotene (Figure 4, H and L). However, at diakinesis or prometaphase I, instead of five bivalents as in the wild type, the mutant contained fewer than five bivalents with the remainder being univalents (Figure 4, Q and U). Among 139 *ptd-1* mutant meiocytes at diakinesis, 128 cells (~92%) had less than five bivalents with the following distributions: four bivalents (21 cells; 15%), three bivalents (50 cells; 36%), two bivalents (32 cells; 23%), one bivalent (16 cells; 12%) and zero bivalents (9 cells; 6%). Among 88 cells counted for *ptd-2*, 87 cells (99%) contained fewer than five bivalents with the following distribution: four bivalents (6 cells; 7%), three bivalents (15 cells; 17%), two bivalents (31 cells; 35%), one bivalent (25 cells; 28%), and zero bivalents (10 cell; 11%). Thus, both *ptd-1* (average bivalents per cell 2.7) and *ptd-2* (average bivalents per cell 1.8) showed a reduced number of bivalents compared with the wild type (average bivalents per cell 5). As mentioned in Azumi *et al*. (2002), the wild-type chromosome interactions and condensation at prophase I has a resemblance to a highly choreographed duet dance in which homologues "dance" in pairs. Because the *ptd* mutant showed the ability to form normal pachytene chromosomes, but then separate at diakinesis, we named the mutants "*parting dancers*," meaning that the chromosomes start the dance as pairs but separate subsequently.

Furthermore, comparison of wild-type and mutant meiocytes at late stages of meiosis I revealed additional defects, which may be a result of the defective prophase I (Figure 4, N–P, R–T, and V–X). In the wild type at meta-

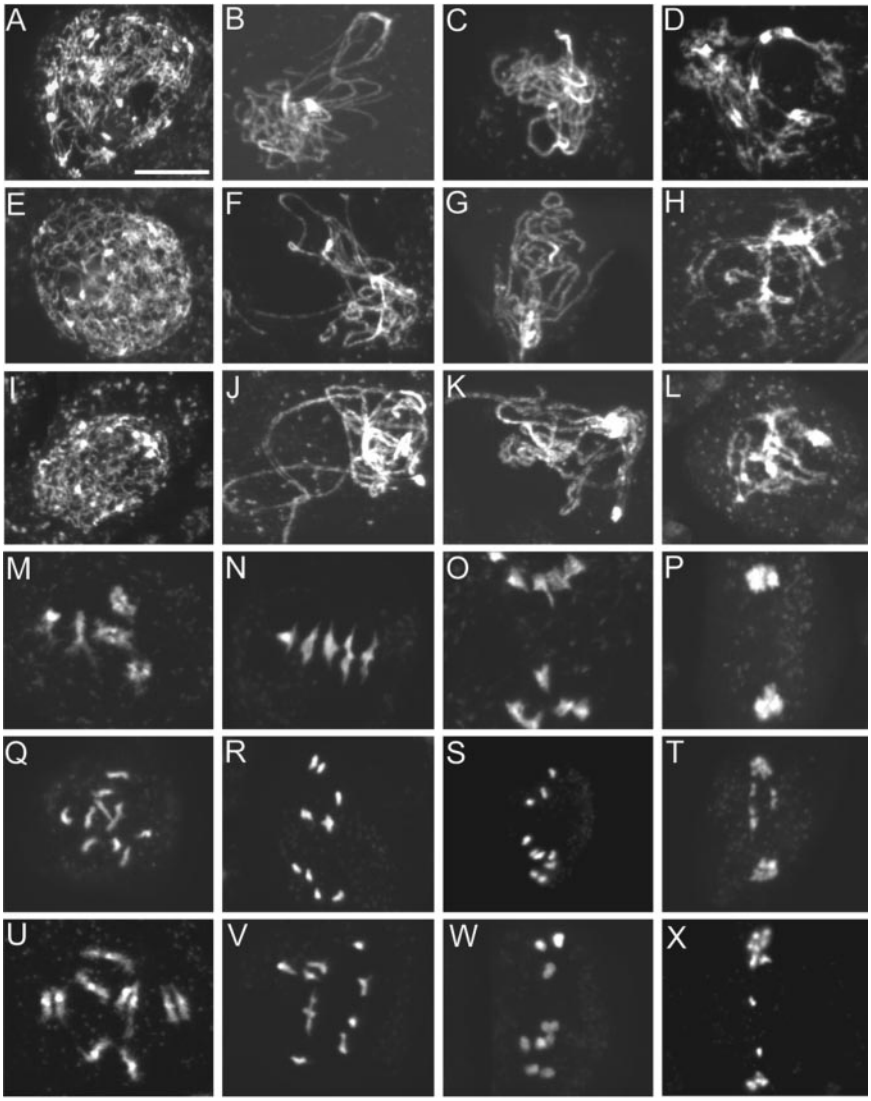

Figure 4. Male meiosis I in the wild type and the *ptd* mutants. Shown are images of DAPI-stained chromosomes. (A–D) Wild-type prophase I at leptotene, zygotene, pachytene, and diplotene, respectively. (E–H) *ptd-1* and (I-L) *ptd-2* prophase I at similar stages showing no obvious difference to the wild type. (M–P) Wild-type diakinesis of prophase I, early metaphase I, anaphase I, and telophase I, respectively; note that M shows five brightly stained entities, representing five attached pairs of condensed homologues. (N) Chromosomes align at the equator. (O) Homologues are separating. (P) Homologues separate and form two clusters. (Q–T) Similar stages of meiosis from *ptd-1*. (U-X) *ptd-2*. Note that in Q, 10 stained bodies can be seen, indicating that the condensed homologues formed univalents. (R and V) Chromosomes condense further, similarly to normal metaphase I chromosomes, but there were no five perfectly aligned bivalents at the equator and contained univalents as in N. Chromosomes are starting to separate similar to (S and W), suggesting that they might be pulled by the spindle as normal homologues are at anaphase I. In T and X, however, the chromosome distribution seems abnormal. Bar, 10 μm.

phase I, the five bivalents are aligned at the equatorial plane of the cell (Figure 4N). At anaphase I, homologous chromosomes separated and migrated toward the two opposite poles (Figure 4O). In contrast, mutant cells with fewer than five bivalents were observed at metaphase I, and cells with five perfectly aligned bivalents were not observed (Figure 4, R and V). In *ptd-1*, among 49 cells at metaphase I, 47 cells (~95%) had fewer than five bivalents with the following distributions: four bivalents (6 cells; 12.2%), three bivalents (12 cells; 24.5%), two bivalents (14 cells; 28.6%), one bivalent (10 cells; 20.4%), and zero bivalents (5 cells; 10.2%). Similarly in *ptd-2*, 47 cells of 47 cells (100%) at metaphase I had fewer than five bivalents with the following distributions: four bivalents (1 cell; 2%), three bivalents (10 cells; 21%), two bivalents (11 cells; 23%), one bivalent (22 cells; 47%), and zero bivalents (3 cells; 6%). Some of the univalents were far from the equator, suggesting that they were not aligned because of the lack of opposing forces from the spindle. The abnormal metaphase I was followed by uneven chromosomal distribution at anaphase I (Figure 4, S and W). In addition, chromosome bridges were observed frequently in the mutant during anaphase I, suggesting possible incomplete recombination.

During wild-type meiosis II, two groups of chromosomes could be observed with a characteristic organelle band in between (Supplemental Figure S1, A–E). At metaphase II the groups of chromosomes (5 in each) assembled at the two equators perpendicular to the organelle band (Supplemental Figure S1, B).The sister chromatids separated and moved to the opposite poles at anaphase II (Supplemental Figure S1, C). Then, the newly formed chromosomes decondensed to form four haploid nuclei (Supplemental Figure S1, D and E). In the mutant meiocytes, chromosome distribution was abnormal, most likely because of the defective prophase I (Supplemental Figure S1, F–O).

The bivalent formation is highly reduced in both *ptd* mutant alleles. Because the majority of the chiasmata in *Arabidopsis* are interference sensitive, it is possible that the *ptd* mutations block the formation of crossovers through the interference-sensitive CO pathway. To test this hypothesis, we counted the distribution of residual chiasmata present in *ptd-1* and *ptd-2* and compared them with that of the wild type (Figure 5). The chiasmata distribution among wild-type

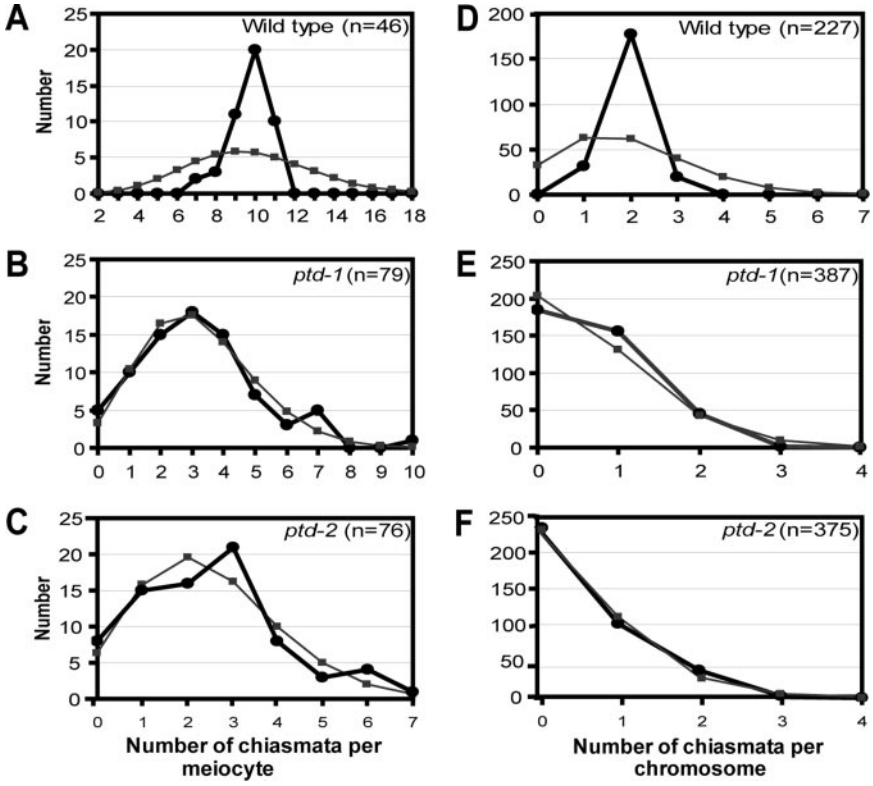

Figure 5. Chiasma distribution in wild type, *ptd-1* and *ptd-2*. (A–C) Chiasma distribution per meiocytes. (D–F) Chiasma distribution per chromosome. Black lines and closed circles indicate observed distributions, whereas gray line and closed squares show predicted Poisson distribution. A and D indicate that the observed distributions of the chiasmata deviate from predicted distributions in the cells and on the chromosome of the wild type, respectively. B, C, E, and F show the observed distributions of the chiasmata do not deviate significantly from the predicted Poisson distributions in mutant cells and on mutant chromosomes.

cells deviated significantly from the Poisson prediction (Figure 5A; $\chi^2_{(18)} = 57.90$, $p < 0.001$), whereas the distribution of the residual chiasmata among cells in both mutant alleles (Figure 5, B and C; *ptd-1*: $\chi^2_{(8)} = 4.16$, $p > 0.7$; *ptd-2*: $\chi^2_{(5)} = 4.22$, $p > 0.5$) did not deviate significantly from the predicted Poisson distribution. In addition, distribution of chiasmata per chromosome in the wild type deviated significantly from the predicted distribution (Figure 5D; wild type $\chi^2_{(8)} = 308$, $p < 0.001$). In contrast, in the *ptd* mutants this distribution was dramatically different from the distribution in the wild type (Figure 5, E and F; *ptd-1*: $\chi^2_{(4)} = 15.472$, $p < 0.05$; *ptd-2*: $\chi^2_{(4)} = 7.895$, $p > 0.05$). This suggested that the majority of the residual chiasmata present in the mutants were randomly distributed and were not sensitive to interference.

Formation of Synaptonemal Complexes and Late Recombination Nodules in ptd

To investigate synapsis in the mutant, we performed TEM analysis on wild-type, *ptd-1* and *ptd-2* meiocytes (Figure 6, A–O). These TEM images revealed no detectable morphological abnormalities in SCs of mutant cells, with properly developed central elements and dimensions that are identical to the wild-type SC (compare Figure 6, E and F, with D and Figure 6, K and L, with J). Pachytene nuclei with fully synapsed chromosomes were observed in both mutant meiocytes. However, delay in formation of SCs in some meiocytes of the mutant was observed. We used the morphology of meiocytes and surrounding tapetal cells to determine the *ptd-1* and *ptd-2* meiocyte stages that corresponded to early or late pachytene in the wild type. All axial elements were assembled into SCs in the wild type at early pachytene (Figure 6A). In *ptd-1*, most axial elements were synapsed, but a few unsynapsed axial elements were also present in the "early pachytene" nuclei (Figure 6B), whereas only short SC stretches were detected in *ptd-2* (Figure 6C). At this stage, most axial elements remained unsynapsed in *ptd-2*, resembling the zygotene stage. In addition, early nodules (ENs) were observed on the central element of SC in both mutant alleles (Figure 6, D–F). During zygotene, 34 ENs were found after examining 44 wild-type serial sections and 22 early nodules from 37 *ptd-2* serial sections. The difference was not statistically significant ($\chi^2_{(1)} = 3.1316$, $p > 0.05$). LNs were also observed on the central elements of SC in *ptd-1* and *ptd-2* as meiosis progressed (Figure 6, G and J, H and K, and I and L). At mid-pachytene, there were 16 LNs on 62 wild-type serial sections and 12 LNs on 67 *ptd* serial sections (not significantly different: $\chi^2_{(1)} = 1.1826$, $p > 0.25$). At late pachytene, we found nine LNs on 45 wild-type sections and eight LNs on 45 *ptd-2* sections (not significantly different: $\chi^2_{(1)} = 0.071$, $p > 0.75$). Furthermore, we did not observe any precocious desynaptic abnormality in the mutant at pachytene. Synaptonemal complexes surrounded with condensed chromatin were regularly seen in late pachytene-early diplotene nuclei in both mutant alleles (compare Figure 6, N and O, with M).

PTD is a Founding Member of Plant Gene Family with Limited Sequence Similarity to ERCC1

The *PTD* gene is predicted to be 2119 base pairs and is located on chromosome 1. *PTD* contains nine exons and eight introns, as supported by the sequence of both our cDNA clone and a reported cDNA (Haas *et al.*, 2002). A 753-base pair *PTD* open reading frame is predicted to encode a 250-amino acid protein with a pI of 9.17 and molecular mass of ~28 kDa. Searches of public databases using BLASTp and PHI-BLASTp revealed no significant overall homology to any other *Arabidopsis* protein but showed a significant sequence similarity to sequences from rice genome that seem to encode a PTD homologue (NCBI accession nos. AAT37994 and AAT44166). This putative homo-

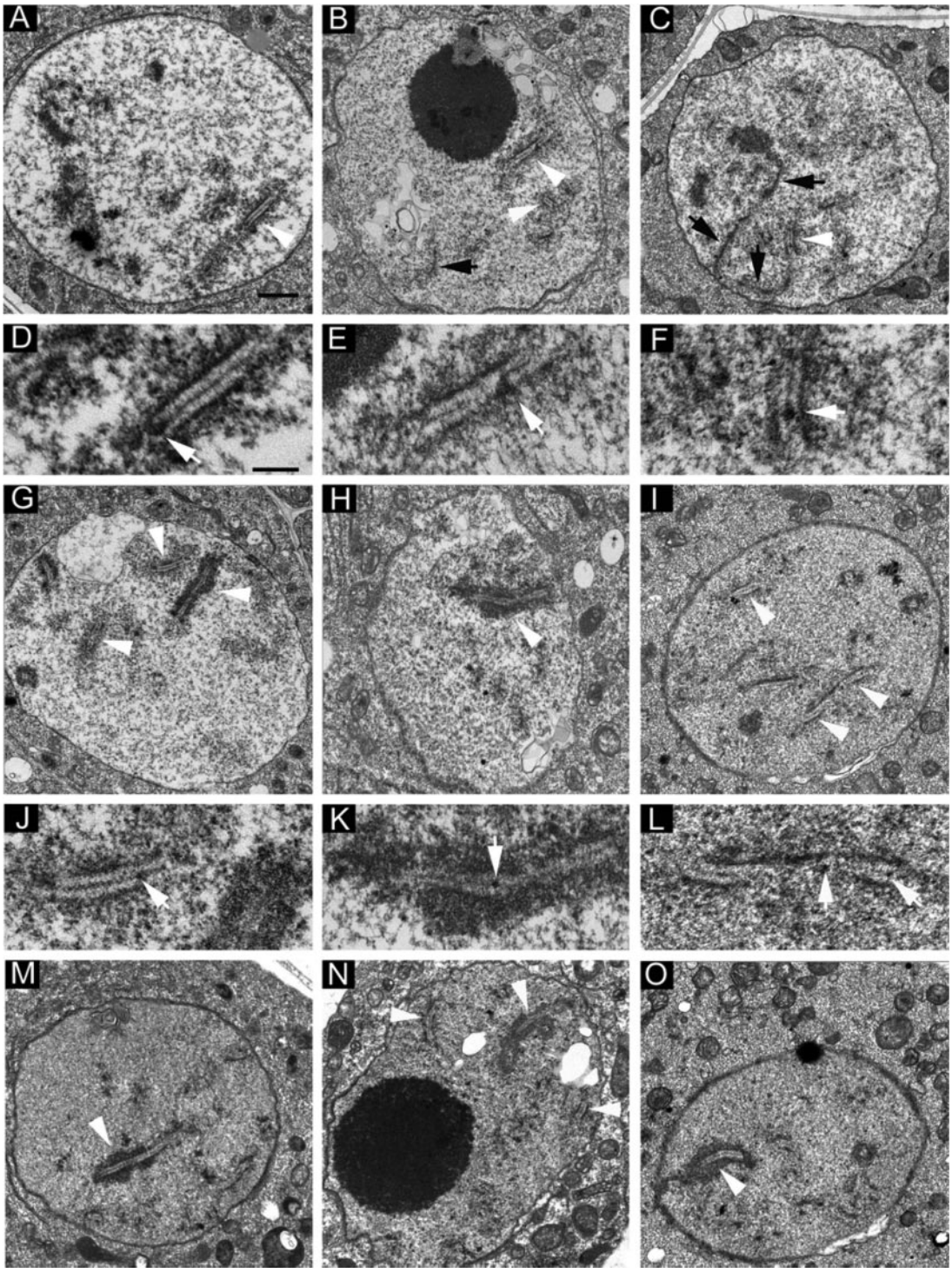

Figure 6. Transmission electron micrographs of wild type (A, D, G, J, and M), the *ptd-1* (B, E, H, K, and N), and the *ptd-2* (C, F, I, L, and O) meiocytes (white arrowheads point to the synaptonemal complexes, black arrows point to unsynapsed elements, and white arrows point to the recombination nodules). (A) Fully synapsed chromosomes in wild type at early pachytene. Almost normal level of synaptonemal complexes in *ptd-1* (B) and reduced level of synaptonemal complexes in *ptd-2* at the same stage (C). Apparently normal level of early recombination nodules in the *ptd-1* and *ptd-2* mutants compared with wild type (A and D, B and E, and C and F). At mid-pachytene in the wild type (G) and *ptd-1* (H), morphology of synaptonemal complex seems identical, but in *ptd-2* development of synaptonemal complexes was delayed (I) (white arrowheads point to synaptonemal complexes). Late recombination nodule on mid-pachytene SC in wild type (J, arrow), in *ptd-1* (K, arrow), and *ptd-2* (L, arrows) at the same stage. Normal level of synaptonemal complexes in both mutant alleles (N, *ptd-1*; O, *ptd*-2) compared with wild type (M) at late pachytene–early diplotene stages. D, E, F, J, K, and L are magnified images from A, B, C, G, H, and I, respectively. Bars, 1000 nm (A–C, G–I, and M–O) and 250 nm (D–F and J–L).

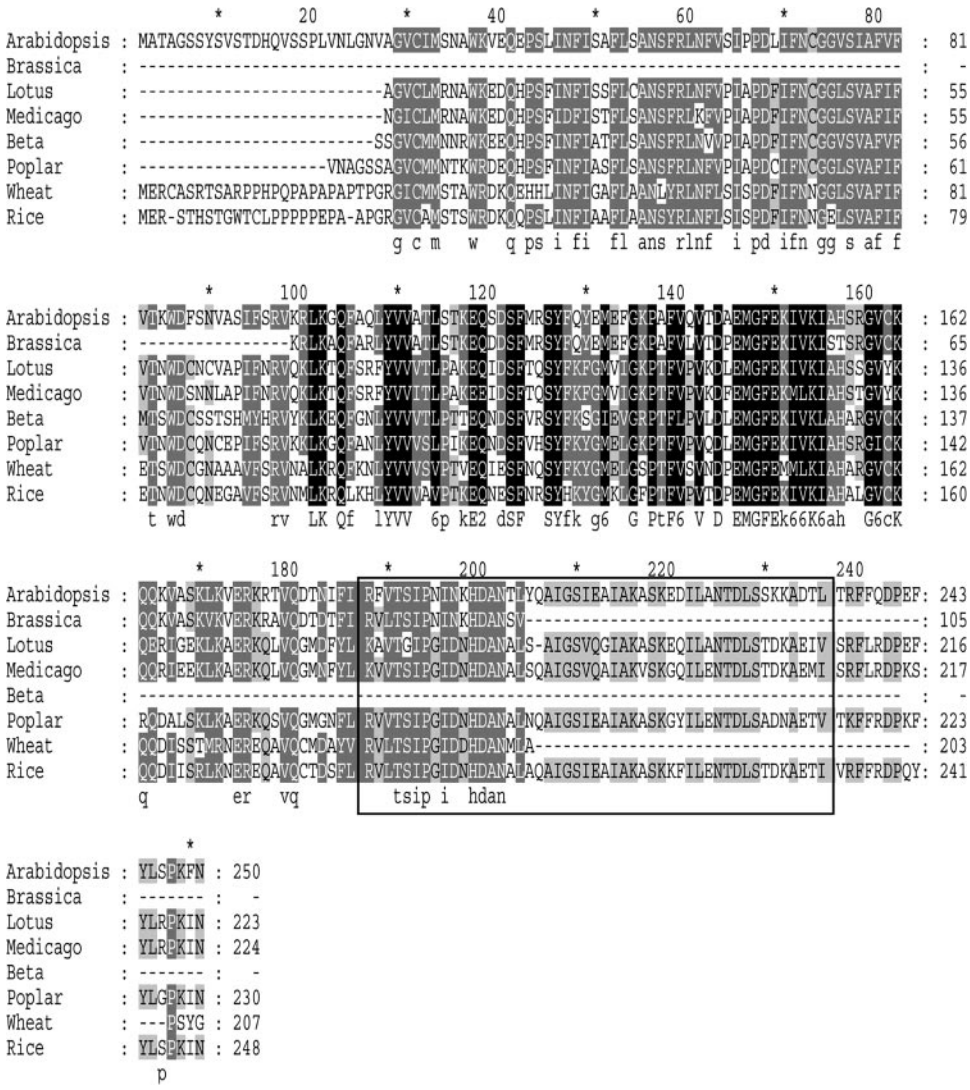

Figure 7. Sequence alignment of PTD homologues in plants. Arabidopsis, *A. thaliana*; Brassica, *Brassica oleracea* (partial EST); Lotus, *Lotus corniculatus*; Medicago, *Medicago truncatula*; Beta, *B. vulgaris* (partial EST); Poplar, *Populus trichocarpa*; Wheat, *Triticum aestivum* (partial EST); and Rice, *Oriza sativa*. Square encloses the putative one pseudo- and one classic HhH motif.

logue, named OsPTD, shared 63% identity and 78% similarity over a 223-aa region with PTD. In addition, there were at least two expressed sequence tag (EST) clones for this rice sequence, indicating that *OsPTD* is expressed (EST, CR288441 and AK109323).

In addition, searches using tBLASTn against National Center for Biotechnology Information nonredundant database for *Lotus corniculatus* (In clone, LjT44D21, TM0127b from 64782 to 66205 bp) and *Medicago truncatula* (In clone, mth2-36b7 from 101727 to 100223) and using JGI (http://genome.jgi-psf.org/Poptr1/Poptr1.home.html) for *Populus trichocarpa* (sequence, LG_I from 30981347 to 30983435) revealed similarity to several genomic sequences (BLAST expected value $2e^{-19}$ and $4e^{-18}$ for *L. corniculatus* and *M. truncatula*, respectively). These genomic sequences were manually annotated using three reading frames generated by Gene Runner software version 3.05 (Hastings Software, Hastings-on Hudson, NY) using PTD and OsPTD amino acid sequences as precursors. In addition, searches against EST databases using tBLASTn yielded several truncated cDNA sequences. One of these is a cDNA from wheat meiotic floret cDNA library that encodes a protein with 51% identity and 67% similarity to PTD over a 217-aa region. Another is a cDNA from developing roots of *Beta vulgaris* that encodes a protein with 65% identity and 79% similarity to PTD over a 135-aa region. A third sequence is from *Brassica* whose predicted protein product has 85% identity and 92% similarity to PTD over a 105-aa region. Therefore, *PTD* is the founding member of a novel gene family in plants. An alignment of the PTD amino acid sequence with representative protein sequences is shown in Figure 7.

Furthermore, the C-terminal region of the PTD protein shares low levels of sequence similarity to several other proteins, including ERCC1 (and its homologues RAD10 and SWI10 from *S. cerevisiae* and *Schizosaccharomyces pombe*, respectively), the UvrC subunit of the ABC exonucleases in bacteria (~24% identities and ~45% similarities in an ~80-aa region) and a bacterial NAD-dependent DNA ligase (36% identity and 58% similarity in a 58-aa region). To obtain clues about the evolutionary relationship between PTD and ERCC1 and XPF, members of the XPF superfamily, we generated a phylogenetic tree using representative sequences from the PTD, ERCC1, and XPF families (protein alignments for construction of the tree is provided in Supplemental Figure S3). This tree showed that putative PTD, ERCC1, and XPF homologues formed three distinct clades, with the ERCC1 and XPF clades represented by members from all major eukaryotic kingdoms and the PTD clade

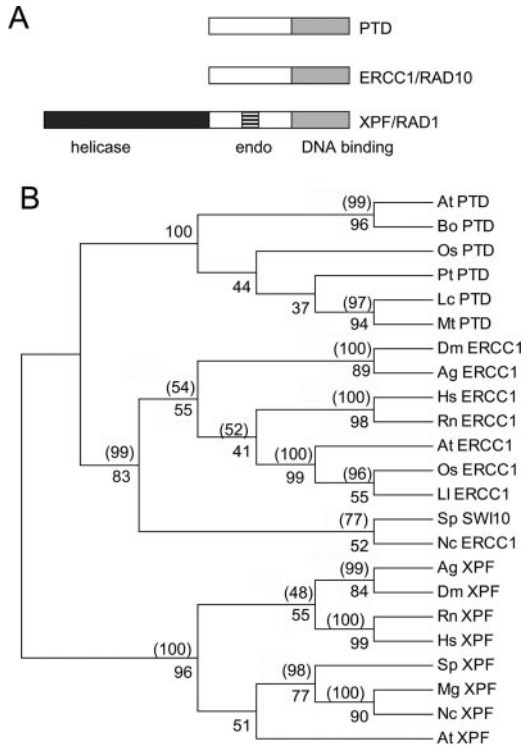

Figure 8. Protein sequence comparison of PTD, ERCC1, and XPF homologues. (A) Schematic representation of protein structure of XPF superfamily members XPF and ERCC1 and PTD. XPF contains an N-terminal helicase domain (helicase), an endonuclease domain (endo), and C-terminal DNA binding domain represented by two HhH motifs. The catalytic domains of XPF share a highly conserved signature motif, GDX_nERKX_3D, that is important for endonuclease activity (Heyer *et al*., 2003; Nishino *et al*., 2003). ERCC1 contains putative endonuclease domain and DNA binding domain with double HhH motifs, but it lacks functionally important residues in its putative catalytic domain (Heyer *et al*., 2003; Tsodikov *et al*., 2005). The PTD proteins possess DNA binding domain similar to ERCC1 but lacks catalytic residues important for endonuclease activity. (B) Maximum parsimony tree for PTD, ERCC1, and XPF homologues in different organisms. Bootstrap (base pairs) values in parentheses indicate base pairs for a tree generated using Neighbor-Joining method for the same sequence alignment. Protein sequences used are as follows: for PTD, *A. thaliana* (At PTD), *B. oleracea* (Bo PTD) (partial EST), *L. corniculatus* (Lc PTD), *M. truncatula* (Mt PTD), *P. trichocarpa* (Pt PTD), and *Oriza sativa* (Os PTD); for ERCC1: *Homo sapiens* (Hs ERCC1), *Rattus norvegicus* (Rn ERCC1), *D. melanogaster* (Dm ERCC1), *Anopheles gambiae* (Ag ERCC1), *S. pombe* (Sp SWI10), *Neurospora crassa* (Nc ERCC1), *A. thaliana* (At ERCC1), *Oryza sativa* (Os ERCC1); and *Lilium longiflorum* (Ll ERCC1); and for XPF, *H. sapiens* (Hs XPF), *R. norvegicus* (Rn XPF), *D. melanogaster* (Dm XPF), *An. gambiae* (Ag XPF), *S. pombe* (Sp XPF), *N. crassa* (Nc XPF), *M. grisea* (Mg XPF), and *A. thaliana* (At XPF).

containing only plant sequences (Figure 8B). In addition, this tree suggests that ERCC1 and PTD are more closely related than they are to XPF.

To gain further insight into the possible function of the PTD protein, its sequence was used to search public databases to identify similar protein domains. Searches in the Protein Families database of alignments and hidden Markov models (Bateman *et al*., 2004) did not identify any known protein domains. In addition, searches in the Simple Modular Architecture Research Tool (SMART) (Letunic *et al*., 2004) database indicated that PTD contains a region (190–234 aa) similar to the Rad51 N-terminal domain; this region in PTD possibly represents one pseudo- and one classic helix-hairpin-helix (HhH) motif. The 190–234-aa region of PTD showed 64–73% aa sequence identities and 77–84% similarities to putative PTD homologues from rice, *P. trichocarpa*, *L. corniculatus*, and *M. truncatula*. In addition, searches against the National Center for Biotechnology Information conserved domain database revealed that a portion of the PTD protein is similar to a domain in the MUS81 protein (37.8%) (Marchler-Bauer *et al*., 2005). However, the low expected value ($2e^{-05}$) and the lack of a functional motif that is characteristic of members of the MUS81 endonuclease family suggest that PTD may not contain a true MUS81 domain. To investigate whether there was any putative subcellular target sequence in PTD, we searched the TargetP database (Emanuelsson *et al*., 2000) and found that PTD did not have any predicted organelle targeting sequence.

DISCUSSION

PTD Is Required for Normal CO Formation and Affects the Interference-sensitive Pathway

Our analysis of two independent *ptd* T-DNA mutants indicates that they are defective in meiotic CO formation. The *ptd* meiocytes have dramatically reduced numbers of chiasmata, which seem to be distributed randomly among cells. We also determined the distribution of chiasmata per chromosome, again with apparently random distribution, in contrast to the interference-sensitive distribution in the wild type. The distribution per chromosome was obtained without knowing the specific chromosome identity because the five *Arabidopsis* chromosomes are hardly distinguishable in DAPI-stained images. Nevertheless, because individual *Arabidopsis* chromosomes do not seem to have a preference for interference-sensitive or interference-insensitive crossovers (Copenhaver *et al*., 2002; Higgins *et al*., 2004; Lam *et al*., 2005), the observed single-chromosome chiasma distributions revealed a real difference between the wild type and the *ptd* mutants. Therefore, the results strongly support the idea that *PTD* is important for the interference-sensitive CO pathway, which requires the *AtMSH4* and *RCK/AtMER3* genes in *Arabidopsis* (Higgins *et al*., 2004; Chen *et al*., 2005; Mercier *et al*., 2005). In the yeast *msh5* and *Arabidopsis atmsh4* mutants, only 10–20% crossovers remain (Börner *et al*., 2004; Higgins *et al*., 2004); however, in *ptd* mutants, the residual chiasmata represent ~30% of the wild-type number per cell (wild type, 9.7 chiasmata per cell; *ptd-1*, 3.2 chiasmata per cell; and *ptd-2*, 2.5 chiasmata per cell). A similar number of residual chiasmata were observed in the *Arabidopsis rck* mutant (32% of the wild-type number) (Chen *et al*., 2005).

The difference in the number of residual chiasmata can be explained by several possible reasons. First, because both alleles produce truncated mRNAs that might encode truncated proteins, the *ptd* alleles might be leaky. In the slightly weaker *ptd-1*, the insertion is in the first exon and the truncated mRNA can potentially encode most of the PTD protein including the C-terminal conserved domain. In *ptd-2*, the insertion is in the fifth exon, leading to a shorter truncated mRNA that would code for a protein lacking the conserved domain. Therefore, *ptd-1* is more likely to have partial function than *ptd-2*. In addition, it is possible that the CO pathway bifurcates downstream of MSH4/MSH5 into two branches, only one of which requires *PTD*. The idea of a bifurcated pathway is also supported by recent studies of the yeast *MLH1* gene (homologue of the bacterial *MutL*), which seems to function downstream of MSH4-MSH5 and may be necessary for only a subset of the *MSH4-MSH5-*

dependent COs (Argueso *et al*., 2004). By analogy, the *Arabidopsis MSH4*-dependent COs may be divided into *PTD*-dependent and *PTD*-independent COs.

PTD Is Not Crucial for Synaptonemal Complex Formation

Recombination and synapsis are closely associated processes; for example, several *Arabidopsis* meiotic recombination mutants also show defects in synapsis (Grelon *et al*., 2001; Li *et al*., 2004; Li *et al*., 2005). In addition, SC formation might initiate at the sites of axial associations, which in yeast may mark future CO sites (Sym *et al*., 1993; Rockmill *et al*., 1995). Yeast mutations in genes encoding synaptonemal initiation complex (SIC) proteins (Fung *et al*., 2004; Page and Hawley, 2004), are defective in formation of both SC and MSH4-MSH5-dependent CO intermediates (Börner *et al*., 2004). Similarly, the *Arabidopsis atmsh4* and *rck/atmer3* mutants exhibit defects in SC formation in addition to reduced CO formation (Higgins *et al*., 2004; Chen *et al*., 2005; Mercier *et al*., 2005). In contrast, the presence of morphologically normal SCs in both *ptd* mutants strongly suggests that PTD functions in the recombination pathway after synapsis has approached completion. Nevertheless, a delay in SC formation in *ptd-2* suggests PTD may have a nonessential role in promoting SC formation.

Another difference between the *ptd* mutants and other mutants defective in CO formation, such as *rck* (Chen *et al*., 2005) or *atrad51* (Li *et al*., 2004), is that the *ptd* mutants had a nearly normal number of late recombination nodules. Recombination nodules are categorized into two types: ENs and LNs. The timing of their appearance and number suggest that EN correspond to the sites of early events where homologue pairing occurs, whereas LNs are associated with the sites of COs (Page and Hawley, 2004; Anderson and Stack, 2005). In addition, there is a close morphological resemblance between LN and SIC and thus LN may be composed of the same SIC proteins, at least in yeast (Page and Hawley, 2004; Anderson and Stack, 2005). The formation of nearly normal numbers of LNs in pachytene meiocytes of the *ptd* mutants suggests that PTD may not be part, nor required for the formation, of the LN complex in pachytene nuclei, unlike AtMSH4 and AtMER3/RCK.

Sequence Similarity of PTD and ERCC1 Suggests a Role for PTD in the Resolution of Meiotic dHJs

The conservation of *PTD* in both monocots and eudicots indicates that the *PTD* gene family had originated before the divergence of these two major angiosperm groups. Our findings suggest that *PTD* function may be conserved in flowering plants, supporting a role for *PTD* in plant meiosis. Whether *PTD* function is also conserved in other eukaryotes, including fungi and animals, is less certain. Nevertheless, an ~80-aa PTD C-terminal region is ~24% identical and ~45% similar to several DNA repair proteins, including ERCC1 (Hoeijmakers, 2001; Sancar *et al*., 2004). It is possible that in nonplant organisms, ERCC1 and related proteins fulfill the meiotic function that in plants requires *PTD*, as supported by the observed CO reduction in *Drosophila mei-9* (affecting an *XPF* homologue) and *ercc1* mutants (Baker and Carpenter, 1972; Sekelsky *et al*., 1995; Radford *et al*., 2005). Conversely, the fact that *PTD* is also expressed widely in many nonmeiotic cells, somewhat similar to a plant *ERCC1* gene (Xu *et al*., 1998), suggests that it may also have a general function, such as DNA repair, as does the *Arabidopsis ERCC1* gene (Hefner *et al*., 2003; Dubest *et al*., 2004).

ERCC1 forms a complex with XPF, and this complex performs a single-strand 5′ incision in DNA nucleotide excision repair and participates in cleavage of in vitro structures that resemble recombinational intermediates (Habraken *et al*., 1994; de Laat *et al*., 1998; Adair *et al*., 2000; Prakash and Prakash, 2000; Sargent *et al*., 2000; Hoeijmakers, 2001; Sancar *et al*., 2004). ERCC1 and XPF are structure-specific endonucleases and are members of the XPF superfamily (Heyer *et al*., 2003; Yang, 2003). In XPF but not ERCC1, a conserved signature motif is important for its endonuclease activity (Enzlin and Scharer, 2002; Nishino *et al*., 2003; Newman *et al*., 2005). Like ERCC1, PTD lacks the XPF signature motif and phylogenetic analysis suggests that PTD is more similar to ERCC1 than to XPF (Figure 8, A and B). Therefore, PTD may act like ERCC1 as a noncatalytic subunit in a complex with another endonuclease to perform a meiotic function (Nishino *et al*., 2003; Newman *et al*., 2005). The *ptd* phenotypes are consistent with the hypothesis that PTD acts downstream of AtMSH4 and RCK/AtMER3, possibly by cutting recombination intermediates, such as dHJ, to complete the process of CO formation. However, PTD may not interact with AtRAD1 (AtXPF) during meiosis because meiotic defects were not detected in the *atrad1* mutant (Liu *et al*., 2000; Dubest *et al*., 2002). Although understanding the mechanism of PTD action needs future studies, the *ptd* phenotypes strongly support its role in CO formation.

ACKNOWLEDGMENTS

We thank to A. Surcel, W. Li, W. Pawlowski, and anonymous reviewers for helpful comments; G. Ning, R. Haldeman, and M. Hazen for assistance in electron microscopy; and A. Omeis, J. Wang, and C. L. Hendrix Hord for plant care. We also thank The Ohio State University *Arabidopsis* Stock Center for providing the SALK and SAIL lines. A.J.W. was partially supported by the Intercollege Graduate Program in Plant Physiology and Department of Biology, The Pennsylvania State University. This work was conducted using material generated with support from the National Science Foundation under Grant 0215923 and was supported by National Institutes of Health Grant R01 GM-63871-01 and National Science Foundation Grant MCB-0092075 (to H. M.). H. M. gratefully acknowledges the generous support of the John Simon Guggenheim Memorial Foundation.

REFERENCES

Adair, G. M., Rolig, R. L., Moore-Faver, D., Zabelshansky, M., Wilson, J. H., and Nairn, R. S. (2000). Role of ERCC1 in removal of long non-homologous tails during targeted homologous recombination. EMBO J. *19*, 5552–5561.

Alexander, M. P. (1969). Differential staining of aborted and nonaborted pollen. Stain Technol. *44*, 117–122.

Alonso, J. M., *et al*. (2003). Genome-wide insertional mutagenesis of *Arabidopsis thaliana*. Science *301*, 653–657.

Anderson, L. K., and Stack, S. M. (2005). Recombination nodules in plants. Cytogenet. Genome Res. *109*, 198–204.

Argueso, J. L., Wanat, J., Gemici, Z., and Alani, E. (2004). Competing crossover pathways act during meiosis in *Saccharomyces cerevisiae*. Genetics *168*, 1805–1816.

Azumi, Y., Liu, D., Zhao, D., Li, W., Wang, G., Hu, Y., and Ma, H. (2002). Homolog interaction during meiotic prophase I in *Arabidopsis* requires the *SOLO DANCERS* gene encoding a novel cyclin-like protein. EMBO J. *21*, 3081–3095.

Baker, B. S., and Carpenter, A. T. (1972). Genetic analysis of sex chromosomal meiotic mutants in *Drosophilia melanogaster*. Genetics *71*, 255–286.

Bateman, A., *et al*. (2004). The Pfam protein families database. Nucleic Acids Res. *32*, D138–D141.

Bishop, D. K., and Zickler, D. (2004). Early decision; meiotic crossover interference prior to stable strand exchange and synapsis. Cell *117*, 9–15.

Bleuyard, J. Y., and White, C. I. (2004). The *Arabidopsis* homologue of *Xrcc3*plays an essential role in meiosis. EMBO J. *23*, 439–449.

Bocker, T., *et al*. (1999). hMSH *5*, a human MutS homologue that forms a novel heterodimer with hMSH4 and is expressed during spermatogenesis. Cancer Res. *59*, 816–822.

Börner, G. V., Kleckner, N., and Hunter, N. (2004). Crossover/noncrossover differentiation, synaptonemal complex formation and regulatory surveillance at the leptotene/zygotene transition of meiosis. Cell *117*, 29–45.

Carpenter, A. T. (1979). Recombination nodules and synaptonemal complex in recombination-defective females of *Drosophila melanogaster*. Chromosoma *75*, 259–292.

Carpenter, A. T. (1982). Mismatch repair, gene conversion, and crossing-over in two recombination-defective mutants of *Drosophila melanogaster*. Proc. Natl. Acad. Sci. USA *79*, 5961–5965.

Celerin, M., Merino, S. T., Stone, J. E., Menzie, A. M., and Zolan, M. E. (2000). Multiple roles of SPO11 in meiotic chromosome behavior. EMBO J. *19*, 2739–2750.

Chen, C., Zhang, W., Timofejeva, L., Gerardin, Y., and Ma, H. (2005). The *Arabidopsis ROCK-N-ROLLERS* gene encodes a homolog of the yeast ATP-dependent DNA helicase MER3 and is required for normal meiotic crossover formation. Plant J. *43*, 321–334.

Colaiacovo, M. P., MacQueen, A. J., Martinez-Perez, E., McDonald, K., Adamo, A., La Volpe, A., and Villeneuve, A. M. (2003). Synaptonemal complex assembly in *C. elegans* is dispensable for loading strand-exchange proteins but not for proper completion of recombination. Dev. Cell *5*, 463–474.

Copenhaver, G. P., Housworth, E. A., and Stahl, F. W. (2002). Crossover interference in *Arabidopsis*. Genetics *160*, 1631–1639.

de Laat, W. L., Appeldoorn, E., Jaspers, N. G., and Hoeijmakers, J. H. (1998). DNA structural elements required for ERCC1-XPF endonuclease activity. J. Biol. Chem. *273*, 7835–7842.

de los Santos, T., Hunter, N., Lee, C., Larkin, B., Loidl, J., and Hollingsworth, N. M. (2003). The Mus81/Mms81 endonuclease acts independently of double Holliday junction resolution to promote a distinct subset of crossovers during meiosis in budding yeast. Genetics *164*, 81–94.

Dernburg, A. F., McDonald, K., Moulder, G., Barstead, R., Dresser, M., and Villeneuve, A. M. (1998). Meiotic recombination in *C. elegans* initiates by a conserved mechanism and is dispensable for homologous chromosome synapses. Cell *94*, 387–398.

de Vries, S. S., Baart, E. B., Dekker, M., Siezen, A., de Rooij, D. G., de Boer, P., and te Riele, H. (1999). Mouse MutS-like protein Msh5 is required for proper chromosome synapsis in male and female meiosis. Genes Dev. *13*, 523–531.

Dubest, S., Gallego, M. E., and White, C. I. (2002). Role of the AtRad1p endonuclease in homologous recombination in plants. EMBO Rep. *3*, 1049–1054.

Dubest, S., Gallego, M. E., and White, C. I. (2004). Roles of the AtERCC1 protein in recombination. Plant J. *39*, 334–342.

Edgar, R. C. (2004). MUSCLE: multiple sequence alignment with high accuracy and high throughput. Nucleic Acids Res. *32*, 1792–1797.

Emanuelsson, O., Nielsen, H., Brunak, S., and Heijne, G. V. (2000). Predicting subcellular localization of proteins based on their N-terminal amino acid sequence. J. Mol. Biol. *300*, 1005–1016.

Enzlin, J. H., and Scharer, O. D. (2002). The active site of the DNA repair endonuclease XPF-ERCC1 forms a highly conserved nuclease motif. EMBO J. *21*, 2045–2053.

Esposito, M. S., and Esposito, R. E. (1969). The genetic control of sporulation in *Saccharomyces*. I. The isolation of temperature-sensitive sporulation-deficient mutants. Genetics *61*, 79–89.

Fung, J. C., Rockmill, B., Odell, M., and Roeder, G. S. (2004). Imposition of crossover interference through the nonrandom distribution of synapsis initiation complexes. Cell *116*, 795–802.

Grelon, M., Vezon, D., Gendrot, G., and and Pelletier, G. (2001). AtSPO11–1 is necessary for efficient meiotic recombination in plants. EMBO J. *20*, 589–600.

Haas, B. J., Volfovsky, N., Town, C. D., Troukhan, M., Alexandrov, N., Feldmann, K. A., Flavell, R. B., White, O., and Salzberg, S. L. (2002). Full-length messenger RNA sequences greatly improve genome annotation. Genome Biol. *3*, RESEARCH0029.

Habraken, Y., Sung, P., Prakash, L., and Prakash, S. (1994). Holliday junction cleavage by yeast Rad1 protein. Nature *371*, 531–534.

Hefner, E., Preuss, S. B., and Britt, A. B. (2003). *Arabidopsis* mutants sensitive to gamma radiation include the homologue of the human repair gene *ERCC1*. J. Exp. Bot. *54*, 669–680.

Heyer, W. D., Ehmsen, K. T., and Solinger, J. A. (2003). Holliday junctions in the eukaryotic nucleus: resolution in sight? Trends Biochem. Sci. *28*, 548–557.

Higgins, J. D., Armstrong, S. J., Franklin, F. C., and Jones, G. H. (2004). The *Arabidopsis* MutS homolog *AtMSH4* functions at an early step in recombination: evidence for two classes of recombination in *Arabidopsis*. Genes Dev. *18*, 2557–2570.

Hillers, K. J. (2004). Crossover interference. Curr. Biol. *14*, R1036–R1037.

Hoeijmakers, J. H. (2001). Genome maintenance mechanisms for preventing cancer. Nature *411*, 366–374.

Hollingsworth, N. M., and Brill, S. J. (2004). The mus81 solution to resolution: generating meiotic crossovers without Holliday junctions. Genes Dev. *18*, 117–125.

Hollingsworth, N. M., Ponte, L., and Halsey, C. (1995). MSH5, a novel MutS homolog, facilitates meiotic reciprocal recombination between homologs in *Saccharomyces cerevisiae* but not mismatch repair. Genes Dev. *9*, 1728–1739.

Housworth, E. A., and Stahl, F. W. (2003). Crossover interference in humans. Am. J. Hum. Genet. *73*, 188–197.

Keeney, S. (2001). Mechanism and control of meiotic recombination initiation. Curr. Top. Dev. Biol. *52*, 1–53.

Keeney, S., Baudat, F., Angeles, M., Zhou, Z. H., Copeland, N. G., Jenkins, N. A., Manova, K., and Jasin, M. (1999). A mouse homolog of the *Saccharomyces cerevisiae* meiotic recombination DNA transesterase Spo11p. Genomics *61*, 170–182.

Kneitz, B., Cohen, P. E., Avdievich, E., Zhu, L., Kane, M. F., Hou, H., Jr., Kolodner, R. D., Kucherlapati, R., Pollard, J. W., and Edelmann, W. (2000). MutS. homolog 4 localization to meiotic chromosomes is required for chromosome pairing during meiosis in male and female mice. Genes Dev. *14*, 1085–1097.

Kumar, S., Tamura, K., and Nei, M. (2004). MEGA *3*, Integrated software for Molecular Evolutionary Genetics Analysis and sequence alignment. Brief. Bioinform. *5*, 150–163.

Kvaratskhelia, M., Wardleworth, B. N., and White, M. F. (2001). Multiple Holliday junction resolving enzyme activities in the Crenarchaeota and Euryarchaeota. FEBS Lett. *491*, 243–246.

Lam, S. Y., Horn, S. R., Radford, S. J., Housworth, E. A., Stahl, F. W., and Copenhaver, G. P. (2005). Crossover interference on nucleolus organizing region-bearing chromosomes in *Arabidopsis*. Genetics *170*, 807–812.

Letunic, I., Copley, R. R., Schmidt, S., Ciccarelli, F. D., Doerks, T., Schultz, J., Ponting, C. P., and Bork, P. (2004). SMART 4. *0*, towards genomic data integration. Nucleic Acids Res. *32*, D142–D144.

Li, W., Chen, C., Markmann-Mulisch, U., Timofejeva, L., Schmelzer, E., Ma, H., and Reiss, B. (2004). The *Arabidopsis AtRAD51*gene is dispensable for vegetative development but required for meiosis. Proc. Natl. Acad. Sci. USA *101*, 10596–10601.

Li, W., Yang, X., Lin, Z., Timofejeva, L., Xiao, R., Makaroff, C. A., and Ma, H. (2005). The *AtRAD51C*gene is required for normal meiotic chromosome synapsis and double-stranded break repair in *Arabidopsis*. Plant Physiol. *138*, 965–976.

Lichten, M. (2001). Meiotic recombination: breaking the genome to save it. Curr. Biol. *11*, R253–R256.

Lilley, D. M., and White, M. F. (2001). The junction-resolving enzymes. Nat. Rev. Mol. Cell. Biol. *2*, 433–443.

Liu, Y., Masson, J. Y., Shah, R., O'Regan, P., and West, S. C. (2004). RAD51C is required for Holliday junction processing in mammalian cells. Science *303*, 243–246.

Liu, Z., Hossain, G. S., Islas-Osuna, M. A., Mitchell, D. L., and Mount, D. W. (2000). Repair of UV damage in plants by nucleotide excision repair: *Arabidopsis* UVH1 DNA repair gene is a homolog of *Saccharomyces cerevisiae* Rad1. Plant J. *21*, 519–528.

Ma, H. (2005). Molecular genetic analyses of microsporogenesis and microgametogenesis in flowering plants. Annu. Rev. Plant Biol. *56*, 393–434.

Marchler-Bauer, A., *et al*. (2005). CDD: a conserved domain database for protein classification. Nucleic Acids Res. *33*, D192–D196.

Mazina, O. M., Mazin, A. V., Nakagawa, T., Kolodner, R. D., and Kowalczykowski, S. C. (2004). *Saccharomyces cerevisiae* Mer3 helicase stimulates 3'-5' heteroduplex extension by Rad51; implications for crossover control in meiotic recombination. Cell *117*, 47–56.

McKim, K. S., and Hayashi-Hagihara, A. (1998). mei-W68 in *Drosophila melanogaster* encodes a SPO11 homolog: evidence that the mechanism for initiating meiotic recombination is conserved. Genes Dev. *12*, 2932–2942.

Mercier, R., Armstrong, S. J., Horlow, C., Jackson, N. P., Makaroff, C. A., Vezon, D., Pelletier, G., Jones, G. H., and Franklin, F. C. (2003). The meiotic protein SWI1 is required for axial element formation and recombination initiation in *Arabidopsis*. Development *130*, 3309–3318.

Mercier, R., *et al*. (2005). Two meiotic crossover classes cohabit in *Arabidopsis*: one is dependent on MER3, whereas the other one is not. Curr. Biol. *15*, 692–701.

Mercier, R., Vezon, D., Bullier, E., Motamayor, J. C., Sellier, A., Lefèvre, F., Pelletier, G., and Horlow, C. (2001). Switch1 (Swi1): a novel protein required for the establishment of sister chromatid cohesion and for bivalent formation at meiosis. Genes Dev. *15*, 1859–1871.

Moffatt, B. A., McWhinnie, E. A., Agarwal, S. K., and Schaff, D. A. (1994). The adenine phosphoribosyl transferase-encoding gene of *Arabidopsis thaliana*. Gene *143*, 211–216.

Nakagawa, T., and Ogawa, H. (1999). The *Saccharomyces cerevisiae MER3* gene, encoding a novel helicase-like protein, is required for crossover control in meiosis. EMBO J. *18*, 5714–5723.

Newman, M., Murray-Rust, J., Lally, J., Rudolf, J., Fadden, A., Knowles, P. P., White, M. F., and McDonald, N. Q. (2005). Structure of an XPF endonuclease with and without DNA suggests a model for substrate recognition. EMBO J. *24*, 895–905.

Nicholas, K. B., Nicholas, H. B., Jr., and Deerfield, D.W.I. (1997). GeneDoc: analysis and visualization of genetic variation. EMBNEW.NEWS *4*, 14.

Nishino, T., Komori, K., Ishino, Y., and Morikawa, K. (2003). X-ray and biochemical anatomy of an archaeal XPF/Rad1/Mus81 family nuclease: similarity between its endonuclease domain and restriction enzymes. Structure *11*, 445–457.

Page, S. L., and Hawley, R. S. (2003). Chromosome choreography: the meiotic ballet. Science *301*, 785–789.

Page, S. L., and Hawley, R. S. (2004). The genetics and molecular biology of the synaptonemal complex. Annu. Rev. Cell Dev. Biol. *20*, 525–558.

Parker, J. L., and White, M. F. (2005). The endonuclease Hje catalyses rapid, multiple turnover resolution of Holliday junctions. J. Mol. Biol. *350*, 1–6.

Petukhova, G., Sung, P., and Klein, H. (2000). Promotion of Rad51-dependent D-loop formation by yeast recombination factor Rdh54/Tid1. Genes Dev. *14*, 2206–2215.

Pochart, P., Woltering, D., and Hollingsworth, N. M. (1997). Conserved properties between functionally distinct MutS homologs in yeast. J. Biol. Chem. *272*, 30345–30349.

Prakash, S., and Prakash, L. (2000). Nucleotide excision repair in yeast. Mutat. Res. *451*, 13–24.

Radford, S. J., Goley, E., Baxter, K., McMahan, S., and Sekelsky, J. (2005). *Drosophila* ERCC1 is required for a subset of MEI-9-dependent meiotic crossovers. Genetics *170*, 1737–1745.

Rockmill, B., Sym, M., Scherthan, H., and Roeder, G. S. (1995). Roles for two RecA homologs in promoting meiotic chromosome synapsis. Genes Dev. *9*, 2684–2695.

Romanienko, P. J., and Camerini-Otero, R. D. (1999). Cloning, characterization, and localization of mouse and human SPO11. Genomics *61*, 156–169.

Ross, K. J., Fransz, P., and Jones, G. H. (1996). A light microscopic atlas of meiosis in *Arabidopsis thaliana*. Chromosome Res. *4*, 507–516.

Ross-Macdonald, P., and Roeder, G. S. (1994). Mutation of a meiosis-specific MutS homolog decreases crossing over but not mismatch correction. Cell *79*, 1069–1080.

Sancar, L. A., Lindsey-Boltz, K., Unsal-Kacmaz, K., and Linn, S. (2004). Molecular mechanisms of mammalian DNA repair and the DNA damage checkpoints. Annu. Rev. Biochem. *73*, 39–85.

Sanchez Moran, E., Armstrong, S. J., Santos, J. L., Franklin, F. C., and Jones, G. H. (2001). Chiasma formation in *Arabidopsis thaliana* accession Wassileskija and in two meiotic mutants. Chromosome Res. *9*, 121–128.

Sanchez-Moran, E., Jones, G. H., Franklin, F. C., and Santos, J. L. (2004). A puromycin-sensitive aminopeptidase is essential for meiosis in *Arabidopsis thaliana*. Plant Cell *11*, 2895–2909.

Sargent, R. G., Meservy, J. L., Perkins, B. D., Kilburn, A. E., Intody, Z., Adair, G. M., Nairn, R. S., and Wilson, J. H. (2000). Role of the nucleotide excision repair gene *ERCC1* in formation of recombination-dependent rearrangements in mammalian cells. Nucleic Acids Res. *28*, 3771–3778.

Sekelsky, J. J., Hollis, K. J., Eimerl, A. I., Burtis, K. C., and Hawley, R. S. (2000). Nucleotide excision repair endonuclease genes in *Drosophila melanogaster*. Mutat. Res. *459*, 219–228.

Sekelsky, J. J., McKim, K. S., Chin, G. M., and Hawley, R. S. (1995). The *Drosophila* meiotic recombination gene *mei-9* encodes a homologue of the yeast excision repair protein Rad1. Genetics *141*, 619–627.

Sessions, A., *et al*. (2002). A high-throughput *Arabidopsis* reverse genetics system. Plant Cell *14*, 2985–2994.

Sijbers, A. M., *et al.* (1996). Xeroderma pigmentosum group F caused by a defect in a structure-specific DNA repair endonuclease. Cell *86*, 811–822.

Snowden, T., Acharya, S., Butz, C., Berardini, M., and Fishel, R. (2004). hMSH4-hMSH5 recognizes Holliday Junctions and forms a meiosis-specific sliding clamp that embraces homologous chromosomes. Mol. Cell *15*, 437–451.

Sung, P., Krejci, L., Van Komen, S., and and Sehorn, M. G. (2003). Rad51 recombinase and recombination mediators. J. Biol. Chem. *278*, 42729–42732.

Sym, M., Engebrecht, J. A., and Roeder, G. S. (1993). ZIP1 is a synaptonemal complex protein required for meiotic chromosome synapsis. Cell *72*, 365–378.

Symington, L. S. (2002). Role of RAD52 epistasis group genes in homologous recombination and double-strand break repair. Microbiol. Mol. Biol. Rev. *66*, 630–670.

Szostak, J. W., Orr-Weaver, T. L., Rothstein, R. J., and Stahl, F. W. (1983). The double strand-break model for recombination. Cell *33*, 25–35.

Tsodikov, O. V., Enzlin, J. H., Scharer, O. D., and Ellenberger, T. (2005). Crystal structure and DNA binding functions of ERCC1, a subunit of the DNA structure-specific endonuclease XPF-ERCC1. Proc. Natl. Acad. Sci. USA *102*, 11236–11241.

Wang, G., Kong, H., Sun, Y., Zhang, X., and Zhang, W. (2004). Genome-wide analysis of the cyclin family in *Arabidopsis* and comparative phylogenetic analysis of plant cyclin-like proteins. Plant Physiol. *135*, 1084–1099.

Xu, H., Swoboda, I., Bhalla, P. L., Sijbers, A. M., Zhao, C., Ong, E. K., Hoeijmakers, J. H., and Singh, M. B. (1998). Plant homologue of human excision repair gene *ERCC1* points to conservation of DNA repair mechanisms. Plant J. *13*, 823–829.

Xu, Y. Y., Chong, K., Xu, Z. H., and Tan, K. H. (2002). Practical techniques of in situ hybridization with RNA probe. Chin. Bull. Bot. *19*, 234–238.

Yang, W. (2003). Pruning DNA: structure-specific endonucleases (XPF/Rad1/Mus81). Structure *11*, 365–366.

Yildiz, O., Kearney, H., Kramer, B. C., and Sekelsky, J. J. (2004). Mutational analysis of the *Drosophila* DNA repair and recombination gene mei-9. Genetics *167*, 263–273.

Yokoyama, H., Kurumizaka, H., Ikawa, S., Yokoyama, S., and Shibata, T. (2003). Holliday junction binding activity of the human Rad51B protein. J. Biol. Chem. *278*, 2767–2772.

Yokoyama, H., Sarai, N., Kagawa, W., Enomoto, R., Shibata, T., Kurumizaka, H., and Yokoyama, S. (2004). Preferential binding to branched DNA strands and strand-annealing activity of the human Rad51B, Rad51C, Rad51D and Xrcc2 protein complex. Nucleic Acids Res. *32*, 2556–2565.

Zar, J. H. (1974). Biostatistical Analysis, Upper Saddle River, NJ: Prentice Hall.

Zhang, X., Feng, B., Zhang, Q., Zhang, D., Altman, N., and Ma, H. (2005). Genome-wide expression profiling and identification of gene activities during early flower development in *Arabidopsis*. Plant Mol. Biol. *58*, 401–419.